The 5th European sCO_2 Conference for Energy Systems
March 14-16, 2023, Prague, Czech Republic

2023-sCO2.eu-115

DYNAMIC SIMULATION AND EXPERIMENTAL VALIDATION OF A 35 MW HEAT PUMP BASED ON A TRANSCRITICAL CO_2 CYCLE

Leonhard Wolscht*
MAN Energy Solutions Schweiz AG
Zurich, Switzerland
Email: Leonhard.wolscht@man-es.com

Kai Knobloch*
Technical University of Denmark
Copenhagen, Denmark
Email: kaikn@dtu.dk

Emmanuel Jacquemoud
MAN Energy Solutions Schweiz AG
Zurich, Switzerland

Philipp Jenny
MAN Energy Solutions Schweiz AG
Zurich, Switzerland

ABSTRACT

Replacing the baseload providers on the energy market with decarbonized renewable solutions increases frequency dynamics on the grid. In order to handle the concomitant risks and chances linked with this change of paradigm between energy producers and consumers, complex dynamic models are required to optimize energy management strategies. Industrial transcritical carbon dioxide (CO_2) heat pumps, such as the one developed by MAN Energy Solutions Schweiz AG (MAN ES), offer a proven solution for the decarbonization of the district heating sector. Furthermore, they are associated with pathways to increase the usage of this solution for sector coupling applications. This work presents a detailed Modelica model of the high-temperature CO_2 heat pump, focusing on the thermodynamic states of the refrigerant during load variations of the system. In a consecutive step, the model is validated against testbed data of a heat pump from MAN ES with over 35 MW heat supply and a lift from 40 to 100 K. The model results match the testbed data with an accuracy of over 95 % and demonstrate a full coverage of the performance map minimum to maximum speed, providing water-side supply temperatures of 50 to 109 °C. Realistic dynamics in fast load balancing operation are demonstrated where power consumption was varied by 80 % compared to maximum power within 30 s. Models of this kind are essential for an accurate prediction how decarbonized energy networks react by linking electricity and heat supply together. These predictions are ultimately useful to upgrade or optimize complex control strategies.

1. INTRODUCTION

Three-quarters of the emissions that have pushed global average temperatures 1.1 °C higher since the pre-industrial age stem from the energy sector [1]. Taking into consideration that the provision of heat for homes and industry accounted for more than half of the total energy consumption in 2021 [2], making it the largest energy end-use, throws into sharp relief the significance of sustainable heat supply for a transition towards a carbon-neutral future [3]. In this context, district heating networks receive particular attention from cities and communities which are leading the energy transition and are increasingly replacing conventional fossil-based heat plants with large-scale heat pumps [4]. Large-scale industrial heat pumps represent an emerging solution for future district energy networks and sector coupling, not only providing heat but also having the potential for cooling applications and ancillary services on the electric grid.

Heat pumps are usually classified according to their working fluid, heat source, temperature level, and physical working principle. Following the work from Lorentzen in 1994 [5], an increasing amount of work investigated CO_2 as a natural refrigerant with low global warming potential, flammability, and toxicity [6]. While large temperature glides in the heat source increase the potential of zeotropic mixtures due to their non-isothermal phase change [7], the high transcritical temperature glide in the gas cooler makes CO_2 particularly suitable for large temperature differences in the heat sink, for example for domestic hot water heating [8]. Unlike ammonia (NH_3) based heat pumps, CO_2 heat pumps can easily achieve sink temperatures above 90 °C and up to more than 130 °C, ideally with heat sink inlet temperatures not too far above the relatively low critical temperature of 31 °C. Moreover, the high volumetric heat capacity of CO_2 allows the use of compact compressors and heat exchangers (HEX) [9]. Besides, using a natural refrigerant like CO_2 for large scale industrial systems reduces environmental and operating risks as well as capital costs compared to synthetic refrigerants or widely used NH_3.

As elaborated in a survey amongst 25 Danish operators and manufacturers of large-scale heat pumps [10], more than 25 %

* joint first and corresponding author(s)

DOI: 10.17185/duepublico/77273

This work may be used under a Creative Commons Attribution 4.0 License.

of the faults during operation are related to the compressor, accounting for the largest share overall and making it the most crucial component of the heat pump system. Additionally, the survey highlights that 38 % of the considered heat pumps are already operating electricity price driven, as well as partly providing ancillary services based on agreements with the utilities.

In conclusion, the key design factors for a district heating heat pump are the selected working fluid and the compressor component. With a focus on these key factors, i) the demonstration of a large-scale system testing with ii) a suitable dynamic model for both, control system and energy management concept, is required. This work presents the dynamic simulation of an industrial high-temperature CO_2 heat pump validated with latest full-scale testbed data from MAN ES.

1.1 Dynamic heat pump modeling

While the first dynamic modeling of heat pumps dating back to the 1980s was using lumped parameter models [11], distributed parameter models, for example, to investigate the dry evaporator for control purposes [12], emerged one decade later.

Already in 1995, Vargas et al. used a mathematical model for a heat pump operating with a variable-speed compressor in a transient regime to propose a closed-loop control (feedback control) instead of the traditional on-off control [13]. Since then, dynamic modeling of heat pumps and their control gained track, ranging from empirical compressor models in heat pumps [14] and performance maps for the entire heat pump [15] to various characteristic maps used to describe each compressor/expander stage individually [16]. However, the ability to provide ancillary services through load variation has only been tested with rapid dynamics on a small scale (kW-scale in seconds [17]) or with moderate dynamics on medium scale (100 s of kW in 1 to 3 minutes [18]).

A large variety of programming and modeling languages is generally used for dynamic modeling of heat pumps, such as Amesim [19], Fortran [9], TRNSYS [20], and Modelica/Dymola [21]. Recently, Modelica based object-oriented model libraries and their application come to the fore due to the availability of commercial simulation environments, with linearization remaining a numerically advantageous and required procedure [22]. Moreover, seminal approaches such as hardware-in-the-loop test benches [23] and reinforcement learning for control optimization [24] seem to have found their common ground in Modelica. Despite the latest advancements, current literature lacks validation on a large scale and for fast operational changes. Dynamic heat pump models are required to fill this gap and are crucial for accurate prediction and design of a variety of emerging application cases including the combination with cold [25] and/or hot [26] thermal storages that could even be used in a successive step for the reconversion to electricity [27].

Figure 1 offers an overview of a general methodology for model-based simulations with the steps presented in this work marked in red.

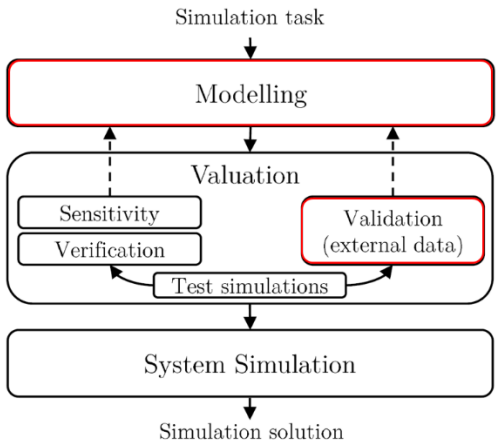

Figure 1 General modeling methodology. In red the steps presented in this work.

After the introduction in section 1, section 2 provides background on the heat pump unit (HPU) layout used for the experimental validation. The modeling part is elaborated on in section 3. Experimental data from a testbed is used to validate the dynamic model in section 4. A general conclusion and an outlook are given in section 5.

2. SYSTEM DESCRIPTION

2.1. HPU Design and Experimental Setup

The HPU layout investigated in this work is a CO_2 transcritical heat pump cycle. Based on the schematic flow diagram in Figure 2, the main components employed and the thermodynamic cycle are illustrated in Figure 3. The multi-stage HOFIM™ radial turbo-compressor (A) brings the CO_2 from a gaseous (1) to a supercritical state (2). In the hot heat exchanger (B), also referred to as the heat sink HEX, heat is transferred to the hot consumer. Still in a supercritical state (3), the CO_2 enters either the turbo-expander (C) or the expander bypass valve (D) where it is expanded into a liquid state (4). A second expansion into the two-phase region takes place across the expansion valve (E). Exiting the expansion valve, the CO_2 mixture at low temperatures (5) is evaporated by heat transfer with a cold consumer through the evaporator heat exchanger (F), also referred to as the heat source HEX.

The core component of the HPU is the high-speed, oil-free integrated motor HOFIM™ compressor which is more compact than conventional compressors, hermetically sealed, and equipped with magnetic bearings. The variable frequency drive allows continuous performance variation over a wide speed range without a gearbox. The motor is cooled with the process medium and reintegrates thermal motor losses into the process.

The selection of both HEXs is mainly determined by the external consumer circuits. The control valves D and E, however, have to be designed to match the turbo-expander. Both valves provide control flexibility to secure that the turbo-expander remains in a single-phase condition and within its pressure-ratio and flow limitations independent from the compressor operation.

DOI: 10.17185/duepublico/77273

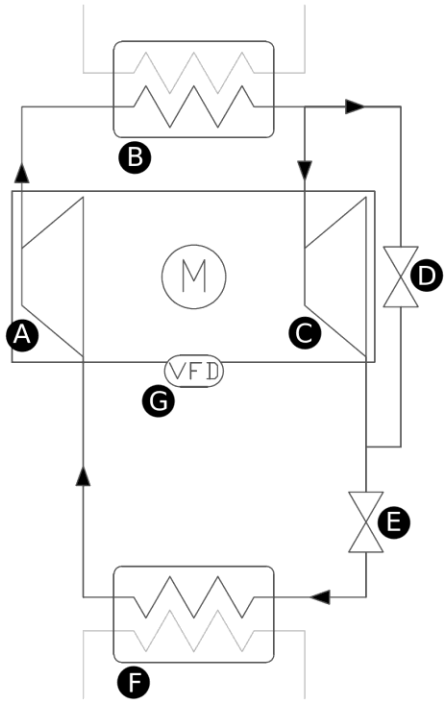

Figure 2: Flow diagram of the HPU. (A) turbo-compressor; (B) hot HEX; (C) turbo-expander; (D) expander bypass valve; (E) expansion valve; (F) evaporator HEX; (G) variable frequency drive.

In 2022, a full-scale HPU prototype was built by MAN ES and tested under various operating conditions. Table 1 gives an informative overview of the process parameters applicable for this kind of experimental setup. Test results have been used to validate the simulation model introduced in Section 4. A picture of the central part of the test setup with the HOFIM™ is shown in Figure 4. The heat sink was integrated using a full-scale printed circuit HEX unit [28] short-circuited with the heat source over several parallel shell-and-tube HEX connected to a water-glycol closed cooling loop. Any surplus of heat was extracted from the water-glycol loop with open air-to-water cooling tower. Redundant piping has been installed for high process flexibility for motor cooling gas flows and is more complex than Figure 2 shows.

For data acquisition, 256 industrial-grade sensors were integrated into the loop, including more than 200 temperature and pressure sensors. Each of the measurement points has been equipped redundantly with double or four-fold sensors to

Table 1: HPU testbed process parameters.

Parameter	Unit	Max. Value
Motor Active Power	MW_{el}	10.5
Heating Duty	MW_{th}	35
Cooling Duty	MW_{th}	25
CO_2 Pressure	bar	140
CO_2 Temperature	°C	130
Min. CO_2 Evaporation Temperature	°C	-2

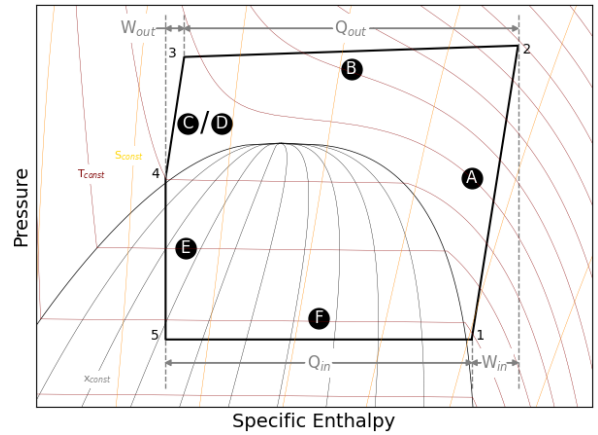

Figure 3: State diagram of CO_2. (1) Superheated gas at compressor suction; (2) hot supercritical state at compressor discharge; (3) cooled supercritical CO2 at expander inlet; (4) liquid state at expander outlet; (5) subcooled liquid and gas mixture (two-phase) at evaporator inlet.

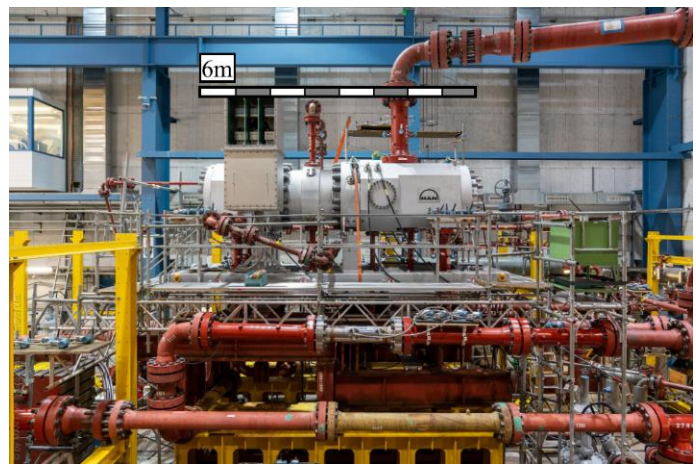

Figure 4: Picture of the turbomachinery part of the testbed setup in MAN ES facility, incl. scale.

minimize measurement errors and risks of hardware failure. The process data is collected via OPC Unified Architecture [29] and is continuously recorded with a sample time of 0.5 Hz.

2.2. Figures of Merit

Turbomachines are described by their characteristic performance maps. This work uses the pressure ratio $\Pi = p_{outlet}/p_{inlet}$ as the work coefficient and the volumetric flow $\dot{v}$ as the flow coefficient spanning a map shown in Figure 6. The performance of both, the compressor and expander, can be expressed in a single point each in their respective characteristic, yielding a compressed comparative value pair containing information on the process conditions at points 1, 2, 3, and 4 of Figure 3 combined. The turbomachine characteristics in this work are based on volume flow instead of reduced mass flow since the compressor is a volumetric machine.

DOI: 10.17185/duepublico/77273

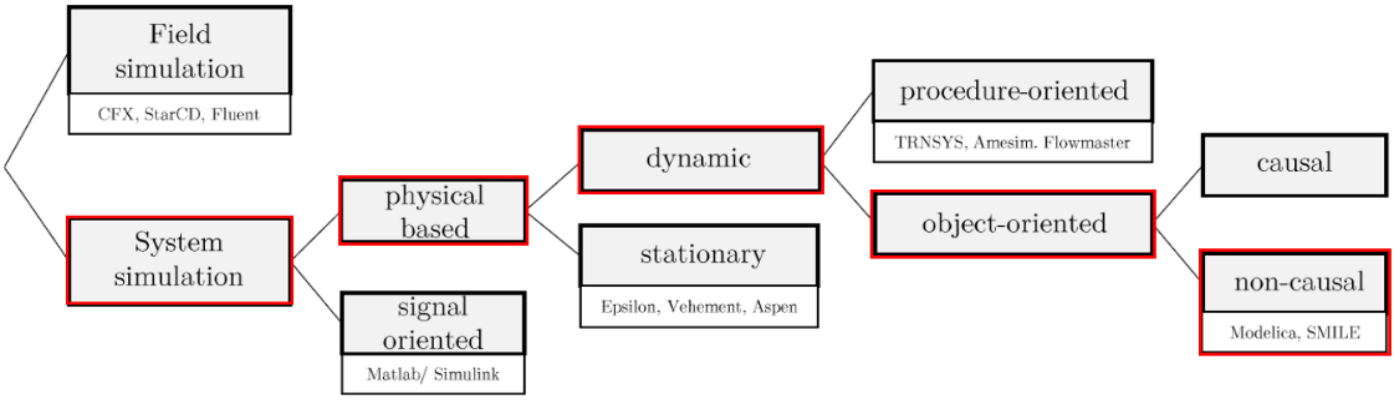

Figure 5: Categorization of simulation approaches (adapted from [30]). In red Modelica as the programming language used here.

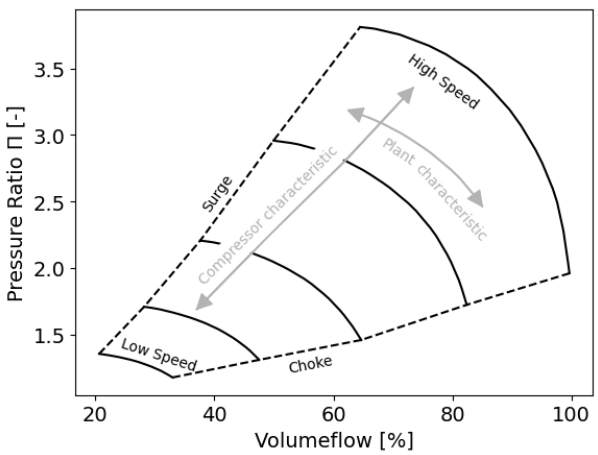

Figure 6: Exemplary characteristic map of a compressor with different lines of constant speed spanning between the choke and surge limit.

Nevertheless, the pressures and temperatures, before and after the compressor, as well as the mass flows at the compressor suction and the motor active power – which is the actual shaft power after the VFD - are more suitable to identify dynamics and shall be referred to as evaluation parameters.

The coefficient of performance (*COP*) is defined based on Figure 3 as

$$COP = \frac{Q_{\mathrm{Out}}}{W_{\mathrm{In}} - W_{\mathrm{Out}}}.$$

The values in Table 1 indicate that the approximate *COP* of the investigated system is roughly 3.3.

For each measured and calculated testbed value, an uncertainty analysis has been performed in order to evaluate the reliability of data and maximum achievable validation accuracy. The acquired data with a sampling time of 0.5 Hz has been grouped and analyzed in sets of one minute. Within this minute, the standard deviation based on mean, minimum, and maximum has been computed and a relative uncertainty to the average data value was calculated. For each test operation, the maximum relative uncertainty of the related minutely datasets has been selected as a maximum confidence interval.

3. MODELLING

3.1. Language and environment

According to the classification by [30], the HPU model is categorized as a non-causal, object-oriented, dynamic, physical-based system simulation, see Figure 5.

The applied object-oriented programming language Modelica is widely used for modeling physical systems. The system components are described by differential-algebraic equations and stored in libraries. The result of the translation is an equation system that is solved by a selected algorithm. One main advantage of Modelica is the multi-domain modeling allowing for the simultaneous modeling and simulation of electric, thermal, mechanic, hydraulic, and pneumatic components. The process-relevant parameters like pressure, temperature, or composition are transferred by connectors between objects. In this context, the acausality of Modelica is worth mentioning. Compared to signal flow oriented software systems like Matlab/Simulink, system circuits are generated faster and in a clear manner. However, some circuit rules need to be considered [31].

In contrast to the programming language Modelica, the simulation environment Modelon Impact used in this work is not open source. In addition to the Modelica Standard Library [32], the modeling in this work is supported by the commercial libraries VaporCycle, ThermalPower, and ThermoFluidPro from Modelon [33].

3.2. Implementation

In preparation for modeling the full HPU, all single components have been validated individually against available datasheets from manufacturers. The full-loop HPU has been composed of the described models in a structure as displayed in Figure 7. Table 2 lists the auxiliary models used, including their underlying physics and associated limitations or advantages, while the main components are explained below.

DOI: 10.17185/duepublico/77273

3.2.1. Medium Model

The media model is based on a spline-based table lookup (SBTL) method. The simulation is much faster compared to the Helmholtz approach which calculates the media properties from equations of state. Especially the stability along the transition between single- and two-phase regions gives the advantage to the table-based approach. Increased speed is achieved by fast access to pre-calculated properties defined in the spline coefficient tables computed with the REFPROP database [34]. Spline coefficient tables are loaded as external objects at the initialization of a simulation. In general, property functions from SBTL (as well as their first derivatives and inverse functions) are continuous and numerically consistent with each other, hence used for various computationally extensive process simulations whenever conventional multi-parameter equations of state are unsuitable due to their computing time consumption, as extensively described by Kunick [35].

3.2.2. Turbomachine Model

The main focus lies on the implementation of the turbomachine as it is the core of the heat pump system. Since the compressor, expander, and motor are physically one unit, there is an individual model for the whole unit. This allows a simple exchange of the turbomachine from the heat pump model and separate validation and testing of the high-speed machine model. As can be seen on the right-hand side close-up in Figure 7, the compressor and expander stream are strictly separated. The compressor is separated into two sections representing different numbers of stages. Each of the turbo machines is described by a table of polytropic efficiency and a flow table. Based on the polytropic head over the model and the impeller tip speed relative to the mediums Mach number, mass flow, torque, and efficiency are computed from 2D tables. While the expander has no leakage streams, the compressor side respects extraction of motor cooling gas over a control valve from between the compressor stages as well as a leakage stream from the high-pressure side into the motor. Motor losses are calculated with a given motor efficiency from the accumulated total shaft power and transferred into the motor cooling stream by a heat flow source.

3.2.3. Heat Exchanger Models

The heat exchangers have been modeled based on the generic model of the Modelon Thermal Power library for two-phase media. It basically represents a pipe-wall-pipe system where pipes can be arbitrarily multiplied and discretized. The heat sink model is discretized into 10 segments, while the heat source model has only 3 segments. The pressure drop over the heat exchangers is calculated based on the friction of a nominal operating point. The heat exchanger model can be fine-tuned with correction factors for both pressure drop and heat transfer. For the hot heat exchanger, the heat transfer correlation of Shah [36] and Akers [37] was used for CO_2.

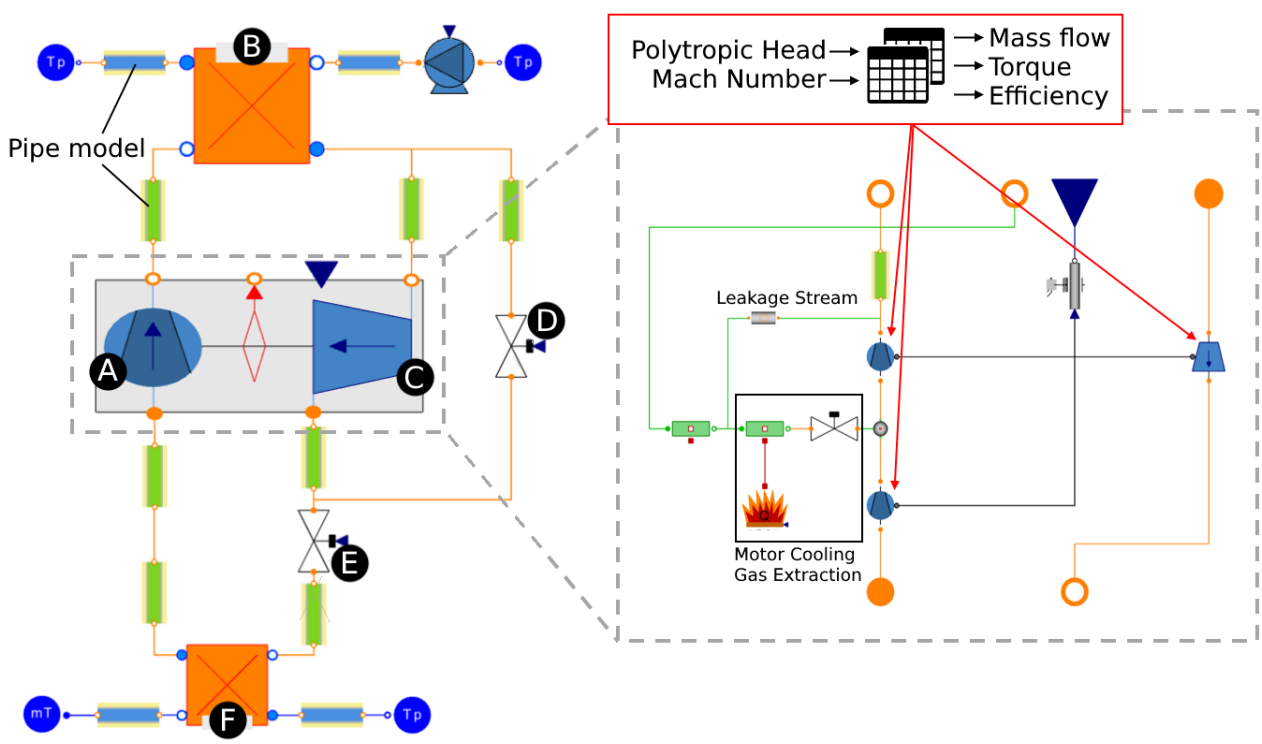

Figure 7: Overview of the HPU in Modelon Impact. The illustrated models correspond to the models described in Subsection 3.2 and Table 2. Please note that detailed piping, control components and cooling gas streams are excluded from this figure.

DOI: 10.17185/duepublico/77273

Table 2: List of used auxiliary models.

Illustration	Description	Limitation
ThermoFluid.Pumps.Pump 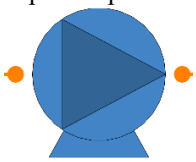	To integrate some control features, this pump model defines the water flow between two pressure sources on the district heating. Characteristics (flow rate, head, and power consumption) are provided in a table for a nominal rotational speed.	• Simplified adaption from nominal conditions with similarity equations. • Speeds outside the table data are extrapolated.
ThermoFluid.Valves.ValveCompressible 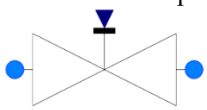	Linear C_v characteristics, following the IEC 534/ISA S.75 standards for sizing including choked conditions.	• Compressible fluid. • Turbulent flow. • No phase change.
VaporCycle.Sources.LiquidPressureSource VaporCycle.Sources.LiquidFlowSource 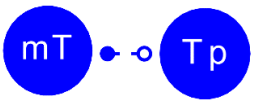	Prescribes an absolute pressure and temperature or a mass flow and temperature, both possible as source or sink.	• Homogeneous liquid. • Temperature and mass fractions set in the component only affect the rest of the system when the component acts as a source.
ThermalPower.Thermal.Sources.HeatFlowSource	A uniform heat flow source converts a power signal input into a heat flow rate.	

3.2.4 Pipe Models

The pipe models of Modelon's VaporCycle library have been manipulated to include a pipe wall and an optional insulation layer as well as an additional flow resistance accounting for all pipe fittings which are not modeled in detail. Pipe elements between major components are represented as straight pipes of constant diameter with a two-phase correlation for friction as proposed by [38] and confirmed for CO_2 by [39]. Additional losses due to fittings such as bends and reductions are summed up into a theoretical resistance factor ζ which imposes

$$dp = \zeta\left(\frac{\rho \cdot v^2}{2}\right).$$

Geostatic height differences between the inflow and outflow of the pipe section are also respected in this model. Heat losses to the environment are included by a constant heat transfer coefficient over the pipe surface to a constant ambient temperature. Pipe models have been parameterized for sections of similar pipe diameter, which results in two consecutive pipe elements at the compressor suction. Short pipe sections such as the framing of the expander bypass valve have been neglected for simplification.

4. VALIDATION

The validity of the dynamic model is tested for the full range of achievable operating conditions which are predominantly defined by the compressor map, see Figure 6. Since the main operational changes in order to move the operating point within the compressor map are identified as the rotational speed of the compressor and the loop resistance, subsection 4.1 and 4.2 compare the model and testbed HPU behavior for large individual changes of these two inputs. While subsection 4.3 validates the simultaneous change of both inputs, the main observations are discussed in subsection 4.4.

4.1 Loop resistance variation

For the validation of system behavior along the plant characteristic, the valve openings have been varied while keeping a constant speed. This variation was performed at the minimum speed (Figures 8, 9, 10) as well as at nominal speed (Figures 9, 11, 12).

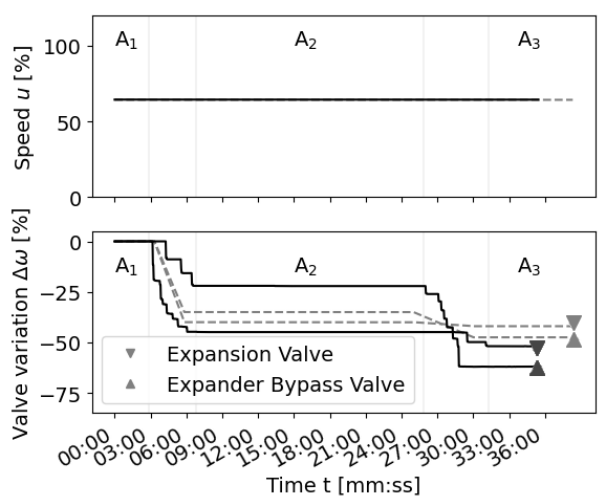

Figure 8: System inputs during the loop resistance variation at low speed by closing the expansion valve; simulated (- -) and testbed data (—).

DOI: 10.17185/duepublico/77273

Figure 8 shows the system inputs. The turbomachine speed was constant at the minimum allowed rotation of 60 % of the nominal speed. The operation starts at the low loop resistance A1 with the expansion valve and expander bypass valve open at 80 and 62 %, respectively. Successively, the valves are shut to a medium resistance point A2 and finally to a high resistance point A3. These three operating points cover most of the compressor's characteristic maps speed line as depicted in Figure 9. Since the characteristic map is composed of multiple stages, it varies with changing suction condition, the indicated surge and choke line can only serve as an orientation, not exact values.

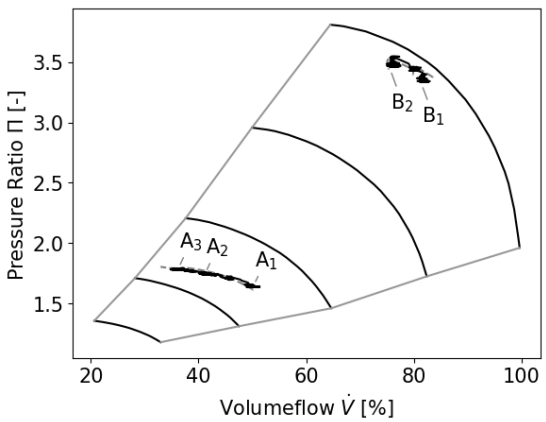

Figure 9: Characteristic compressor map during the low- (A) and high-speed (B) loop resistance variation; simulated (- -) and testbed data (—).

Figure 10 compares the main physical quantities of the simulation and testbed data. The simulated compressor performance, temperatures, and mass flow are more than 95 % accurate (based on the system inputs from Figure 8).

For nominal speed, the allowed resistance variation was limited due to testbed restrictions of the cooling water system. The valve variation is therefore constrained to a slight closing of the expansion valve as shown in Figure 11 and results in only a small movement in the theoretical characteristic map from Figure 9. The agreement between simulation and testbed results in Figure 12 is consistently satisfactory over every parameter with an accuracy of 95 %. The testbed data uncertainty during these rather slow dynamics is below 2 % throughout all data points.

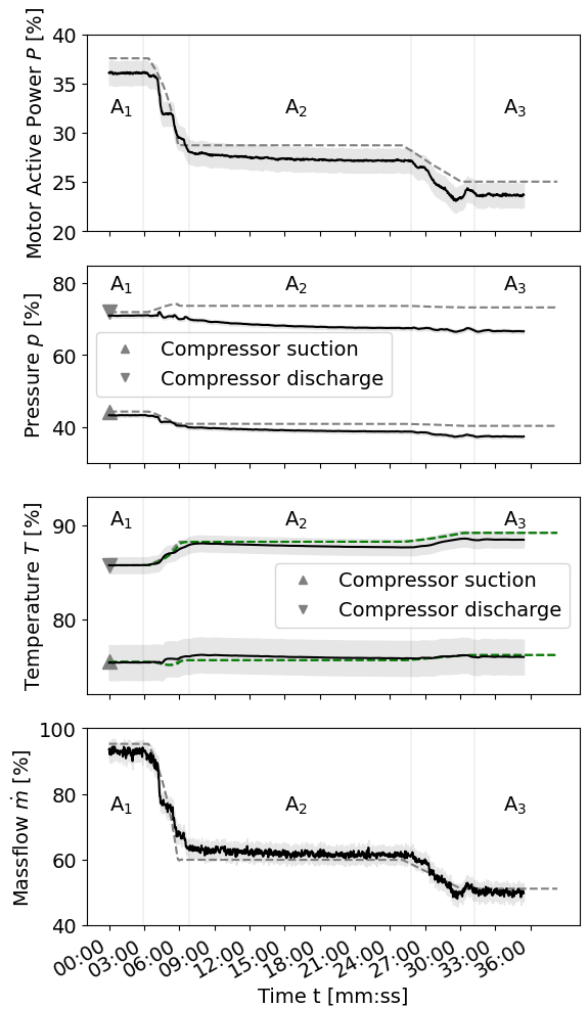

Figure 10: Physical quantities during the low-speed loop resistance variation; simulated (- -) and testbed data (—) with a confidence interval (■) as defined in subsection 2.2. Results of adding a time delay on the simulation output of the temperature are plotted in green.

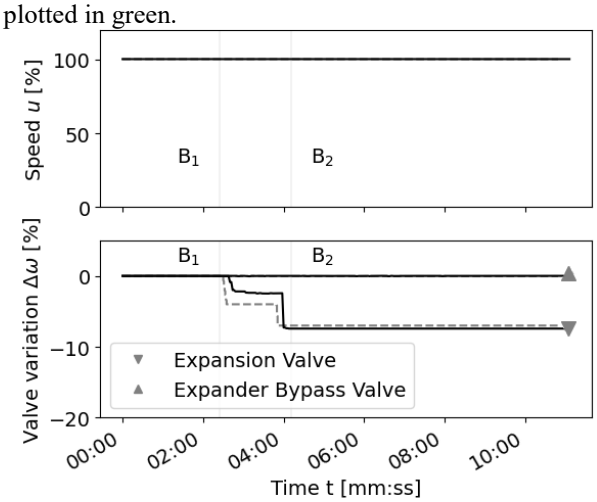

Figure 11: System inputs during the loop resistance variation at high speed by closing the expansion valve; simulated (- -) and testbed data (—).

DOI: 10.17185/duepublico/77273

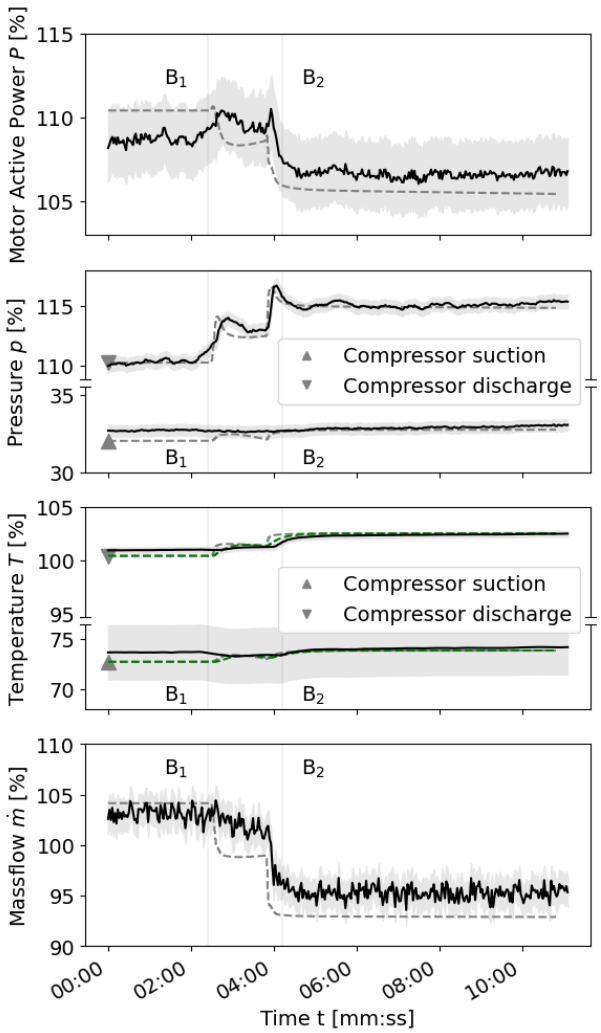

Figure 12: Physical quantities during the high-speed loop resistance variation; simulated (- -) and testbed data (—) with a confidence interval (■) as defined in subsection 2.2. Results of adding a time delay on the simulation output of the temperature are plotted in green.

4.2 Rotational speed variation

In order to validate the system behavior along the compressor characteristic (see Figure 6), the speed was varied rapidly while keeping all other parameters (e.g. valves, water temperatures) constant, imitating a primary frequency reserve operation on European markets [40]. In Figure 13, the speed as input in the simulation and testbed procedure is shown. From nominal speed, at 100 %, the rotation of the turbomachine shaft was reduced to 60 % within 30 s and restored after a settle-out period of 50 s. Similarly, a speed variation increasing from nominal to 105 % was performed.

While the transient dynamics demonstrate high accuracy, the visualization in the characteristic compressor map in Figure 14 suffers mainly from the smallest deviations in absolute pressure measurements. Both curves resemble an 8-shape where the larger, lower loop is related to the speed decrease operation 100 %-60 %-100 % and the much smaller, upper loop is caused by the speed increase operation 100 %-105 %-100 %.

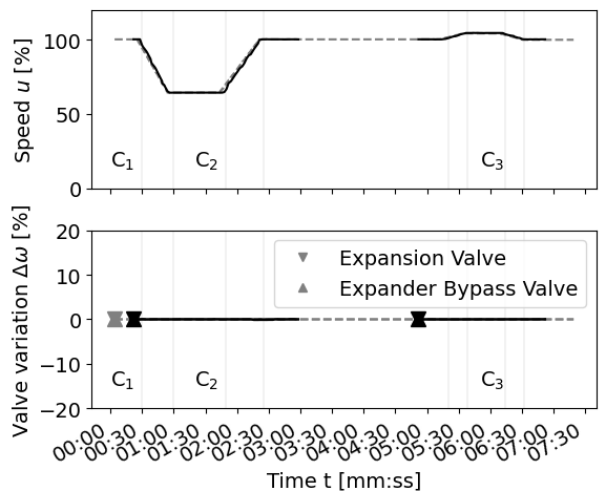

Figure 13: System inputs during the high-speed loop resistance variation; simulated (- -) and testbed data (—).

The power consumption of the HPU – as a result – falls to 26 % of the nominal duty. The transient dynamics are in good agreement between the simulation and testbed system, showing only a small deviation when settling after the large speed increase from 60 % to nominal. A similar agreement can be found in the fluid state measurements as presented in Figure 15. The transient behavior is captured well in absolute numbers and dynamics. A larger deviation is found in the temperature, where the dynamics of the simulation are much quicker than what testbed data shows. Adding a first-order transfer function with a delay of 15 s to the simulation temperature data yields the green result and much better agreement with the testbed measurements.

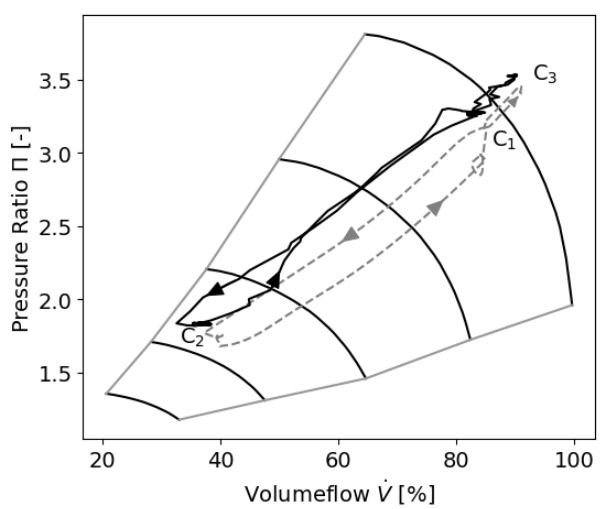

Figure 14: Characteristic compressor map during the speed variation; simulated (- -) and testbed data (—).

DOI: 10.17185/duepublico/77273

The testbed measurements show a high uncertainty of up to 20% for mass flow and temperatures during these fast dynamics. Generally, it is concluded that the simulation results show a good qualitative agreement with the testbed data. Over wide ranges, especially during steady states, the quantitative values also reach a high accuracy of more than 95 %. Several result deviations are discussed in subsection 4.4.

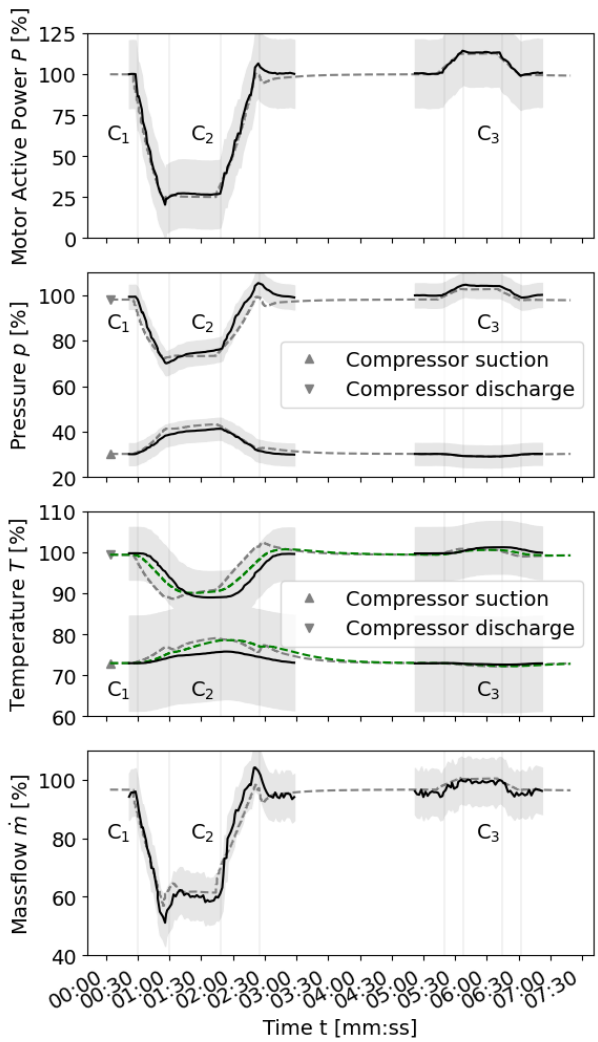

Figure 15: Physical quantities during the speed variation; simulated (- -) and testbed data (—) with a confidence interval (■) as defined in subsection 2.2. Results of adding a time delay on the simulation output of the temperature are plotted in green.

4.3 Combined variation of rotational speed and loop resistance

After the validation of transient operation with a single input variation, the response of a simultaneous change of both, speed and valve position, is investigated. A fast load-balancing operation is performed, reducing the speed by 60 % within 30 s and at the same time opening both valves, expansion and expander bypass, as given in Figure 16.

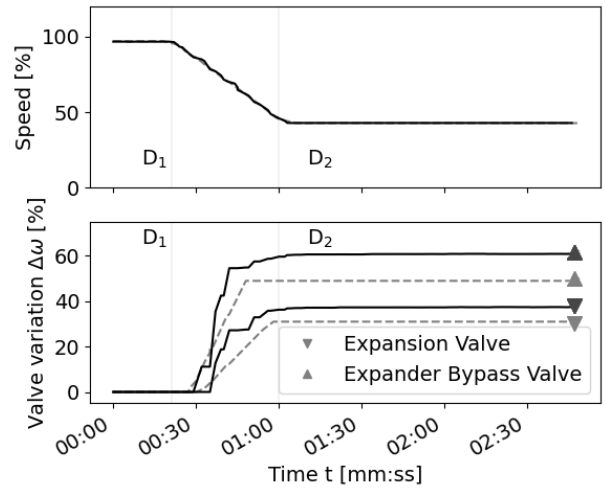

Figure 16: System inputs during the speed as well as loop resistance variation; simulated (- -) and testbed data (—).

Figure 17 shows the transition in the characteristic map. The operating point moves diagonally from a high-speed point at high resistance to a minimum speed closer to the choke line. A slight offset of the simulation is present again, but the shape of the path is in good agreement between experimental data and simulation.

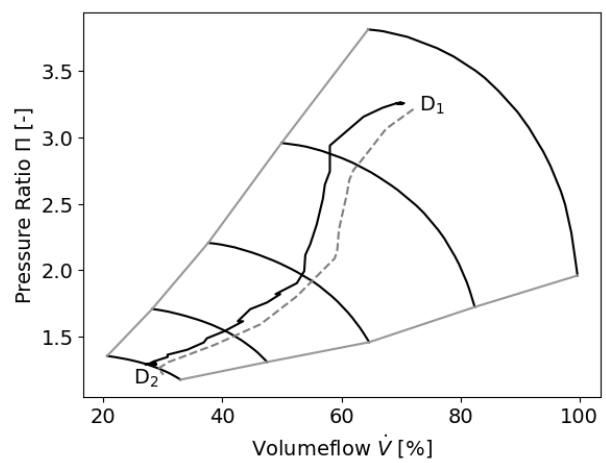

Figure 17: Characteristic compressor map during the speed as well as loop resistance variation; simulated (- -) and testbed data (—).

The power consumption of the testbed HPU falls by over 80 % within 45 s and is well matched by the simulation. Also, compressor pressures, temperatures, and mass flow remain in agreement with the experimental data in highly dynamic transitions as shown in Figure 18. As seen above, the hot temperature measurement on the compressor discharge is delayed on the testbed but can be compensated with an imposed time delay to the simulation output.

DOI: 10.17185/duepublico/77273

Table 3: Summary of the most relevant observations together with potential causes as well as proposed measures.

Observation (corresponding subsection)	**Root**	**Measure**
Pressure drift for slow dynamics (4.4.1)	Thermal shift on the water-glycol loop impacts the evaporation pressure	None – physical testbed limitation
Loop resistance uncertainties (4.4.2)	Simplified pipe modeling, challenging valve characteristics	Linear valve model based on testbed or improved manufacturer data
Elevated testbed path in the characteristic compressor map (4.4.3)	Overperformance of the manufactured compressor (conservative compressor model)	Regenerate compressor maps based on testbed measurements
Temperature deviations (4.4.4)	Thermal inertia of temperature sensors	Implementation of first-order transfer function(s)
High sensitivity to total CO_2 mass (4.4.5)	Inaccurate mass balance measurement on the testbed	None – physical testbed limitation

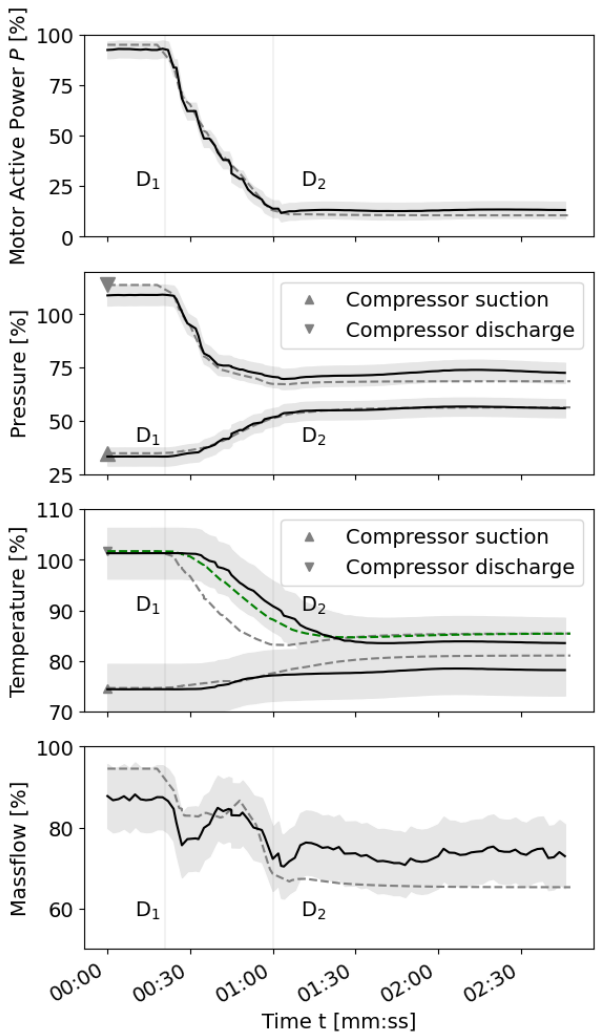

Figure 18: Physical quantities during the speed as well as loop resistance variation; simulated (--) and testbed data (—) with a confidence interval (■) as defined in subsection 2.2. Results of adding a time delay on the simulation output of the temperature are plotted in green.

4.4 Discussion of the results

The most relevant observations during the validation, together with their root and potential measures, are summarized in Table 3 as well as elaborated in the following subsections.

4.4.1 Pressure drift for slow dynamics

In Figure 10, a strong pressure drift, defined as a gradual, unintended deviation of the process from the expected performance, can be observed. This unsteady drift can be linked to challenges in manually adjusting the cooling water flow in the testbeds interlinked heat sink and source. Balancing the thermal energy of the testbed loop is complex and results in a thermal shift on the evaporator. This directly influences the evaporation pressure and can project to all of the closed-loop states. Further, this limitation of the interlinked heat sink and source also restricts the loop resistance variation at high speeds, resulting in the rather short path in Figure 9.

4.4.2 Loop resistance uncertainties

Another major discrepancy between the simulation and testbed is the overall loop resistance, visible in the deviating valve positions throughout all validation cases in Figures 8, 11, 13, and 16. A fundamental cause lies in the simplifications of pipe modeling. Additional pipes and armatures on the testbed as well as varying surface conditions on different pipe elements and a high number of flange connections are difficult to model accurately. On top of this comes the poor quality of the valve characteristics. In ever-changing fluid properties from liquid to multiphase to supercritical and even gaseous states, the correlation between opening, C_v, and actual resistance is non-trivial. The choice of a simple linear valve model in correspondence with the manufacturer is a conscious decision to allow for tuning flexibility on the loop resistance. While a fitting valve opening can be easily found based on measurement data, it limits the control application of the model at this stage to qualitative use only.

DOI: 10.17185/duepublico/77273

4.4.3 Elevated testbed path in the compressor map

The paths of the testbed and the simulation data in the characteristic map for the load-balancing operation are slightly shifted. The data translation into pressure ratio emphasizes small deviations and measurement inertia on the testbed projects onto the volume flow. In Figure 14 the simulation gives a nearly ideal path, while the path of the testbed data appears morphed. On one hand, this is caused by a fast pressure measurement and a comparably slow temperature sensor which results in a temporarily wrong combination of data points. The dominating shift of the experimental data to higher pressure ratios is explained by a conservative compressor model. The manufactured compressor wheels reach higher pressures than designed for a given volume flow. The compressor look-up tables should be recalculated and updated based on the testbed experience.

4.4.4 Temperature deviations

The dynamic response of the temperature differs significantly between the simulation results in the dotted gray and the testbed results in solid black as described in section 4.2 and is visible in Figure 15 and Figure 18. By adding a first-order transfer function with a time constant of 15 s to the temperature output of the simulation, the resulting temperature curve in dotted green is in much better agreement. This could be explained by the thermal inertia of the temperature sensors, which had not been in direct contact with the medium but placed in an insertion sleeve, leading to a delay. The impact of measurement inertia is non-negligible and contributes to the systematic validation uncertainty. Especially computed values from the testbed such as volume flow, enthalpy and ultimately *COP* propagate this error and inhibit a higher uncertainty during transient operation.

4.4.5 Total refrigerant charge

It is challenging to accurately monitor the total mass of refrigerant present in the test loop. Therefore, it can only be roughly estimated based on weight inventory measurements during the charging procedure. Moreover, some refrigerant was added or removed during the multiple days of testing, resulting in significant uncertainties of the refrigerant charge at a certain time. The actual refrigerant mass varied in the range between 5.5 to 6.5 tons. This relatively large uncertainty creates, however, a degree of freedom for the simulation which can have an impact on the results.

5. CONCLUSION

Large-scale industrial heat pumps are crucial solutions for the decarbonization of district energy networks or process heat applications. An optimal integration in complex operating frameworks must take into consideration the system dynamics. Hence, transient simulation is one of the key tools to provide accurate predictions of future heat pump operation. More specifically, application services such as seasonal load planning, day-to-day heat balancing, and highly dynamic grid services can be supported by the concept and tool elaborated in this work. The presented model improves on the current state-of-the-art by its validation with full-scale experimental testing results. For fast self-induced operational changes, the major results can be summarized as follows:

- The developed Modelica HPU model matches the testbed measurements with an accuracy of 95 % in the discussed physical quantities (with few exceptions as discussed).
- Fast dynamic changes of the power consumption up to 80 % within 30-45 s by varying the loop resistance and the speed have been validated both, individually and combined.
- The validated HPU model is qualified to predict transient plant operation and control responses.

As the next step of development, the integration of elaborated valve characteristics can provide dynamic models for even more accurate system predictions. Besides ensuring the scalability of such models, future studies should investigate control strategies on different time scales. A validated dynamic model as presented here can serve as the foundation for more complex energy management systems connecting long-term resource planning with fast dynamics of ancillary services on an industrial scale.

NOMENCLATURE

CO_2	Carbon Dioxide
COP	Coefficient of Performance
C_v	Valve Flow Coefficient
ρ	Density [kg/m^3]
dp	Pressure Loss [Pa]
HEX	Heat Exchanger
HPU	Heat Pump Unit
IEC	International Electrotechnical Commission
ISA	International Society of Automation
MAN ES	MAN Energy Solutions Schweiz AG
NH_3	Ammonia
SBTL	Spline-based Table Lookup
$Q_{in/out}$	Specific Heat [J/kg]
v	Median Flow Velocity [m/s]
$W_{in/out}$	Specific Work [J/kg]
ζ	Flow Resistance Factor [-]

CREDIT AUTHOR STATEMENT

Leonhard Wolscht Conceptualization, Data curation, Software, Model, Writing, Visualization **Kai Knobloch** Conceptualization, Data curation, Software, Writing, Visualization, Funding acquisition **Emmanuel Jacquemoud** Resources, Supervision, Writing - Review **Philipp Jenny** Writing - Review.

DOI: 10.17185/duepublico/77273

ACKNOWLEDGMENTS

The authors would like to express their gratitude to MAN Energy Solutions Schweiz AG for supporting this work with resources as well as experimental data. Kai Knobloch acknowledges the financial support from the Danish Energy Technology Development and Demonstration Program (EUDP 64016-0027) and the Otto Mønsteds Fund. The authors would like to thank Christian Hermsdorf, George Kleynhans, Zeno Antonini, and Luis Sanz Garcia for their valuable engineering expertise and support.

REFERENCES

[1] International Energy Agency. World Energy Outlook. Paris; 2021.
[2] International Energy Agency. Heating. Paris; 2021.
[3] van Vuuren DP, van Soest H, Riahi K, Clarke L, Krey V, Kriegler E et al. Carbon budgets and energy transition pathways. Environ. Res. Lett. 2016;11(7):75002.
[4] International Energy Agency. District Heating. Paris; 2021.
[5] Lorentzen G. Revival of carbon dioxide as a refrigerant. International Journal of Refrigeration 1994;17(5):292–301.
[6] Gabrielli P, Sansavini G, Singh S, Garcia LS, Jacquemoud E, Jenny P. Off-Design Modeling and Operational Optimization of Trans-Critical Carbon Dioxide Heat Pumps. Journal of Engineering for Gas Turbines and Power 2022;144(10).
[7] Zühlsdorf B, Jensen JK, Cignitti S, Madsen C, Elmegaard B. Analysis of temperature glide matching of heat pumps with zeotropic working fluid mixtures for different temperature glides. Energy 2018;153:650–60.
[8] Arpagaus C, Bless F, Uhlmann M, Schiffmann J, Bertsch SS. High temperature heat pumps: Market overview, state of the art, research status, refrigerants, and application potentials. Energy 2018;152:985–1010.
[9] Diniz HAG, Paulino TF, Pabon JJG, Maia AAT, Oliveira RN. Dynamic Model of a Transcritical CO2 Heat Pump for Residential Water Heating. Sustainability 2021;13(6):3464.
[10] Aguilera JJ, Meesenburg W, Ommen T, Poulsen JL, Kramer KR, Markussen WB et al. Operational challenges in large-scale ammonia heat pump systems. In: Amano Y, Sciubba E, Elmegaard B, editors. 34th International Conference on Efficiency, Cost, Optimization, Simulation and Environmental Impact of Energy Systems (ECOS 2021). Tokyo, Japan: ECOS 2021 Program Organizers; 2022, p. 1842–1853.
[11] Chi J, Didion D. A simulation model of the transient performance of a heat pump. International Journal of Refrigeration 1982;5(3):176–84.
[12] Nyers J, Stoyan G. A dynamical model adequate for controlling the evaporator of a heat pump. International Journal of Refrigeration 1994;17(2):101–8.
[13] Vargas J, Parise J. Simulation in transient regime of a heat pump with closed-loop and on-off control. International Journal of Refrigeration 1995;18(4):235–43.
[14] Dechesne B, Bertagnolio S, Lemort V. Development of an empirical model of a variable speed vapor injection compressor used in a Modelica-based dynamic model of a residential air source heat pump. IOP Conf. Ser.: Mater. Sci. Eng. 2015;90:12031.
[15] Thomasen S, Sørensen K, Bojesen C, Vinther K. Sensitivity Analysis of Optimised Large Scale District Heating Heat Pump Concepts. In: Proceedings of The 61st SIMS Conference on Simulation and Modelling SIMS 2020, September 22-24, Virtual Conference, Finland: Linköping University Electronic Press; 2021, p. 63–70.
[16] Thermal Power Library - Experiments - HeatPump: Example of a MW-scale, two-stage district heating heat pump system based on R134a: Modelon Inc; 2022.
[17] Kim Y-J, Norford LK, Kirtley JL. Modeling and Analysis of a Variable Speed Heat Pump for Frequency Regulation Through Direct Load Control. IEEE Trans. Power Syst. 2015;30(1):397–408.
[18] Meesenburg W, Markussen WB, Ommen T, Elmegaard B. Optimizing control of two-stage ammonia heat pump for fast regulation of power uptake. Applied Energy 2020;271:115126.
[19] Watanabe Y, Traverso A. Dynamic modeling and simulation of a heat pump system for enhancing cycle flexibility. E3S Web Conf. 2019;113:1007.
[20] Byrne P, Miriel J, Lenat Y. Design and simulation of a heat pump for simultaneous heating and cooling using HFC or CO2 as a working fluid. International Journal of Refrigeration 2009;32(7):1711–23.
[21] Ko J, Takata N, Thu K, Miyazak T. Dynamic Modeling and Validation of a Carbon Dioxide Heat Pump System. Evergreen 2020;7(2):172–94.
[22] Gräber M, Kosowski K, Richter C, Tegethoff W. Modelling of heat pumps with an object-oriented model library for thermodynamic systems. Mathematical and Computer Modelling of Dynamical Systems 2010;16(3):195–209.
[23] La Tejeda De Cruz A, Riviere P, Marchio D, Cauret O, Milu A. Hardware in the loop test bench using Modelica: A platform to test and improve the control of heating systems. Applied Energy 2017;188:107–20.
[24] Peirelinck T, Ruelens F, Decnoninck G. Using reinforcement learning for optimizing heat pump control in a building model in Modelica. In: 2018 IEEE International Energy Conference (ENERGYCON): IEEE; 2018, p. 1–6.
[25] Selvnes H, Allouche Y, Hafner A. Experimental characterisation of a cold thermal energy storage unit with a pillow-plate heat exchanger design. Applied Thermal Engineering 2021;199:117507.
[26] Knobloch K, Muhammad Y, Costa MS, Moscoso FM, Bahl C, Alm O et al. A partially underground rock bed

 DOI: 10.17185/duepublico/77273

thermal energy storage with a novel air flow configuration. Applied Energy 2022;315:118931.
[27] Vecchi A, Knobloch K, Liang T, Kildahl H, Sciacovelli A, Engelbrecht K et al. Carnot Battery development: A review on system performance, applications and commercial state-of-the-art. Journal of Energy Storage 2022;55:105782.
[28] Le Pierres R, Southall D, Osborne S. Impact of Mechanical Design Issues on Printed Circuit Heat Exchangers. Proceedings of sCO2 Power Cycle Symposium 2011.
[29] OPC Foundation. The Industrial Interoperability Standard™.
[30] Gerhard S. Energy storages: Presentation during the International Joint Graduate Course on Sustainable Energy. Seoul.
[31] Wischhusen S. Dynamische Simulation zur wirtschaftlichen Bewertung von komplexen Engergiesystemen. 1st ed. Göttingen: Cuvillier; 2005.
[32] Modelica Association. Modelica Standard Library 3.2.1.
[33] Modelon Inc. Modelon Library Suite 2022.
[34] Huber M, Harvey A, Lemmon E, Hardin G, Bell I, McLinden M. NIST Reference Fluid Thermodynamic and Transport Properties Database (REFPROP) Version 10 - SRD 23: National Institute of Standards and Technology; 2018.
[35] Kunick M. Fast Calculation of Thermophysical Properties in Extensive Process Simulations with the Spline-Based Table Look-Up Method (SBTL): VDI Verlag; 2018.
[36] Shah MM. A general correlation for heat transfer during film condensation inside pipes. International Journal of Heat and Mass Transfer 1979;22(4):547–56.
[37] Akers, W.W., Deans, H.A., Crosser, O.K. Condensing heat transfer within horizontal tubes. Chem. Eng. Progr. 1959(55).
[38] Friedel L. Improved friction pressure drop correlations for horizontal and vertical two-phase pipe flow. Proceedings of European Two-Phase Flow Group Meeting;1979(2).
[39] Park CY, Hrnjak PS. CO2 and R410A flow boiling heat transfer, pressure drop, and flow pattern at low temperatures in a horizontal smooth tube. International Journal of Refrigeration 2007;30(1):166–78.
[40] ENTSO-E. European association for the cooperation of transmission system operators (TSOs) for electricity; Available from: https://www.entsoe.eu/.

DOI: 10.17185/duepublico/77273

DuEPublico

Duisburg-Essen Publications online

UNIVERSITÄT DUISBURG ESSEN

Offen im Denken

ub | universitäts bibliothek

Published in: 5th European sCO2 Conference for Energy Systems, 2023

This text is made available via DuEPublico, the institutional repository of the University of Duisburg-Essen. This version may eventually differ from another version distributed by a commercial publisher.

DOI: 10.17185/duepublico/77273
URN: urn:nbn:de:hbz:465-20230427-111604-6

This work may be used under a Creative Commons Attribution 4.0 License (CC BY 4.0).